Lipid partitioning at the nuclear envelope controls membrane biogenesis

Antonio Daniel Barbosa[a], Hiroshi Sembongi[a,*], Wen-Min Su[b], Susana Abreu[c], Fulvio Reggiori[c], George M. Carman[b], and Symeon Siniossoglou[a]
[a]Cambridge Institute for Medical Research, University of Cambridge, Cambridge CB2 0XY, United Kingdom; [b]Department of Food Science and the Rutgers Center for Lipid Research, New Jersey Institute for Food, Nutrition and Health, Rutgers University, New Brunswick, NJ 08901; [c]Department of Cell Biology, University Medical Center Groningen, University of Groningen, 9713 A Groningen, Netherlands

ABSTRACT Partitioning of lipid precursors between membranes and storage is crucial for cell growth, and its disruption underlies pathologies such as cancer, obesity, and type 2 diabetes. However, the mechanisms and signals that regulate this process are largely unknown. In yeast, lipid precursors are mainly used for phospholipid synthesis in nutrient-rich conditions in order to sustain rapid proliferation but are redirected to triacylglycerol (TAG) stored in lipid droplets during starvation. Here we investigate how cells reprogram lipid metabolism in the endoplasmic reticulum. We show that the conserved phosphatidate (PA) phosphatase Pah1, which generates diacylglycerol from PA, targets a nuclear membrane subdomain that is in contact with growing lipid droplets and mediates TAG synthesis. We find that cytosol acidification activates the master regulator of Pah1, the Nem1-Spo7 complex, thus linking Pah1 activity to cellular metabolic status. In the absence of TAG storage capacity, Pah1 still binds the nuclear membrane, but lipid precursors are redirected toward phospholipids, resulting in nuclear deformation and a proliferation of endoplasmic reticulum membrane. We propose that, in response to growth signals, activation of Pah1 at the nuclear envelope acts as a switch to control the balance between membrane biogenesis and lipid storage.

INTRODUCTION

Cell growth and proliferation require phospholipids, the major building blocks of membranes, and survival during nutritional deprivation depends on energy stored in the form of triacylglycerols (TAGs). Because phospholipids and TAG share common precursors, cells must spatially and temporally control the flow of lipids toward growth or storage in a nutrient-dependent manner. The mechanisms responsible for this coordination within the endoplasmic reticulum membrane (ER) network, where lipid synthesis takes place, are poorly understood. Such mechanisms are crucial for proper growth control and metabolic homeostasis in healthy individuals, and their disruption underpins the development of cancer, type 2 diabetes, and obesity.

TAGs, together with esterified sterols, are deposited in ubiquitous organelles—lipid droplets (LDs; Pol *et al.*, 2014). During LD biogenesis, cells coordinate synthesis of TAG from glycerol and fatty acids through a series of acylation steps, with the expansion of the emerging LD from the ER membrane. Phosphatidate (PA), a key intermediate in the pathway (Figure 1A), is dephosphorylated to diacylglycerol (DAG) by Mg^{2+}-dependent PA phosphatases (PAPs; Pascual and Carman, 2013). Subsequent fatty acid acylation of DAG by acyltransferases (DGATs) generates TAG (Yen *et al.*, 2008). Because the size and number of LDs vary widely between cell types and growth stage, homeostatic mechanisms coordinating LD biogenesis with nutritional or developmental status must be in place, but these are largely unknown.

PA is also a central precursor for the synthesis of phospholipids. Therefore the PAP reaction is a key branching step that commits glycerol backbones and fatty acids for TAG synthesis. Budding yeast

FIGURE 1: Nutrient-dependent targeting of Pah1 to a subdomain of the nuclear envelope. (A) Schematic of the main lipid biosynthetic pathways that control membrane growth vs. storage. Dashed arrows indicate pathways that channel DAG to phospholipids. The Kennedy pathway directly channels DAG to phospholipids (bottom dashed arrow). (B) Left, growth curve of the cells imaged in C. Optical density (OD_{600}) at which growth deceleration and the transitions in Pah1*-GFP targeting take place. Right, neutral lipid levels during growth. Cells were labeled with BODIPY 493/503, and fluorescence was quantified as described in *Material and Methods*. Data are representative of four independent repeats. (C) Wild-type cells expressing the indicated fusion proteins and labeled with MDH to visualize LDs were grown from exponential phase (Exp) to the indicated densities and imaged live. Arrowheads point to intermediates where Pah1*-GFP is both on NVJ and LD. Arrows point to Pah1*-GFP on the nuclear membrane flanking the NVJ at later

expresses one PAP enzyme that is essential for TAG synthesis, Pah1 (Han et al., 2006), whereas mammals express three PAPs, lipins 1–3 (Peterfy et al., 2001; Donkor et al., 2007). Rodent models of lipin 1 deficiency display a lipodystrophic phenotype, characterized by significant reduction in fat mass and lack of adipocyte differentiation (Csaki et al., 2013). Of note, unlike other enzymes of the TAG biosynthetic pathway, Pah1 and lipins lack transmembrane domains and therefore must first translocate onto membranes in order to generate DAG. This step is inhibited by multisite phosphorylation, mediated by Pho85, Cdc28, and protein kinase A in yeast (Choi et al. 2011, 2012; Su et al., 2012) and target of rapamycin (TOR) and mitotic kinases in mammals (Huffman et al., 2002; Harris et al., 2007; Grimsey et al., 2008). Dephosphorylation of Pah1 is catalyzed by the highly conserved transmembrane Nem1-Spo7 complex (Siniossoglou et al., 1998; Santos-Rosa et al., 2005) and is required for Pah1 membrane recruitment and activation (O'Hara et al., 2006; Karanasios et al., 2010; Choi et al., 2011).

Of interest, in addition to their TAG storage defects, pah1Δ mutants display a reciprocal increase in membrane biogenesis at the ER that results in a striking expansion of the nuclear membrane, suggesting that Pah1 regulation may be also important for nuclear envelope remodeling (Santos-Rosa et al., 2005; Siniossoglou, 2009). Similar nuclear defects were described in fission yeast cells lacking the Pah1 orthologue Ned1 (Tange et al., 2002), whereas a role for lipins in nuclear envelope dynamics and nuclear morphology has been also established in worms and mammals (Gorjánácz and Mattaj, 2009; Golden et al., 2009; Mall et al., 2012; Bahmanyar et al., 2014).

Despite the progress on the protein factors that regulate Pah1, the physiological signals that drive this enzyme to its membrane-bound form and the identity of the ER compartment(s) where it is activated have remained elusive. Given the critical position of Pah1 in lipid synthesis, in this study, we set out to test the hypothesis that growth and nutrient signals during starvation control Pah1 targeting to membranes and determine the site where Pah1-mediated lipid partitioning takes place.

RESULTS
Nutritional control of Pah1 targeting mediates LD biogenesis at a nuclear membrane subdomain
To test whether Pah1 activation on membranes drives lipid flux toward storage, we first examined targeting of Pah1 in time-course experiments during growth in glucose. Pah1–green fluorescent protein (GFP) detection has been hindered by its low expression levels and protein instability due to proteasome-mediated degradation of the activated enzyme (Pascual et al., 2014). This prompted us to use a Pah1-GFP fusion carrying the D398A D400A mutations within its DXDX(T/V) catalytic motif (hereafter referred to as Pah1*-GFP). This mutant binds membranes without dephosphorylating PA (Karanasios et al., 2010) and is more stable than the wild-type enzyme (Pascual et al., 2014). To avoid the severe effects of loss of Pah1 activity in cell

morphology and growth, all experiments using Pah1*-GFP described here were performed in cells expressing the endogenous Pah1.

During exponential phase and the presence of ample glucose, Pah1*-GFP exhibits a diffuse cytoplasmic distribution (98 ± 1% cells), consistent with continued phospholipid production for sustaining biomass accumulation. After the deceleration of growth due to glucose exhaustion at the diauxic shift (post–diauxic shift [PDS]) phase (see growth curve in Figure 1B), Pah1*-GFP targeted transiently the nuclear membrane domain that contacts the vacuole (nuclear vacuole junction [NVJ]; Figure 1, C–E). Subsequently, Pah1*-GFP concentrated to two nuclear membrane puncta flanking the NVJ that were in contact with LDs (Figures 1, C and D; Supplemental Figure S1). We observed that Pah1*-GFP was in contact with the DAG acyltransferase Dga1, but did not entirely colocalize with it (Supplemental Figure S2). During the NVJ-to-LD transition, we noticed a discontinuous thread of Pah1*-GFP labeling that connected with adjoining LD-associated pools, suggesting that the NVJ pool of Pah1 gradually concentrates in the proximity of LDs (Figure 1C, arrowheads). Of importance, the most significant increase of neutral lipids coincides with the translocation of Pah1*-GFP to the nuclear membrane–LD interface (Figure 1, B and C). This suggests that a nutrient-sensing signal targets Pah1 to the nuclear membrane, ensuring that lipid intermediates are diverted from phospholipid synthesis into storage lipids. Of interest, murine lipin 2–GFP showed a similar growth-dependent targeting to the nuclear membrane–LD interface when expressed in pah1Δ cells (Figure 1F).

The NVJ is established by the physical interaction of Nvj1 (on the perinuclear ER) and Vac8 (on the vacuolar membrane; Pan et al., 2000). The only known function of the NVJ is in the piecemeal microautophagy of the nucleus (PMN), where nonessential portions of the nucleus and nuclear membrane are degraded. Evidence for a lipid-remodeling event during PMN is provided by the presence of other lipid metabolic enzymes at the NVJ (Kvam et al., 2007) and the fact that a liquid disordered microdomain reporter, Vph1-mCherry, is excluded from the NVJ during PMN (Toulmay and Prinz, 2013; Dawaliby and Mayer, 2010). We find that Pah1*-GFP recruitment to the NVJ coincides with the exclusion of Vph1-mCherry in the PDS phase (Supplemental Figure S3). Therefore Pah1 might have a role in lipid remodeling in order to promote PMN.

To determine the role of NVJ in the recruitment of Pah1 to the nuclear envelope, we imaged Pah1*-GFP in the nvj1Δ mutant. We found that when Pah1*-GFP localizes to the NVJ in wild-type cells (4 < OD_{600} < 6), it maintains a diffuse soluble distribution in nvj1Δ cells. However, at later stages (6 < OD_{600} < 8), Pah1*-GFP still localized to a punctum onto the nuclear membrane in 88 ± 3% of the nvj1Δ cells (Figure 1G). Moreover, at this stage, neutral lipid or TAG levels did not decrease in nvj1Δ (Supplemental Figure S4). Thus the targeting of Pah1 to the nuclear membrane and its function in TAG storage do not require the NVJ.

stages. The star indicates the vacuole, identified by its autofluorescence. (D) Quantification of the Pah1*-GFP relocalization shown in C. Two hundred cells from three independent experiments were scored. (E) Colocalization of Pah1*-GFP with Nvj1-mCherry during the exit from exponential growth. Wild-type cells (RS453) expressing a chromosomally integrated Nvj1-mCherry and Pah1*-GFP were grown as in B and C and imaged at an OD_{600} of 4.1. The outline of the cell is depicted, and the position of the vacuole (vac) indicated. (F) Lipin 2 targets the nuclear membrane–associated LD pool. pah1Δ cells expressing lipin2-GFP and the indicated reporters were grown to the post–diauxic shift (PDS) phase and imaged by epifluorescence microscopy using a Zeiss Axioplan microscope. (G) Targeting of Pah1*-GFP to the nuclear envelope in the nvj1Δ mutant. Cells expressing the indicated fusion proteins were grown to an OD_{600} of 7.2 and imaged as in C. Scale bar, 5 μm (C, E–G).
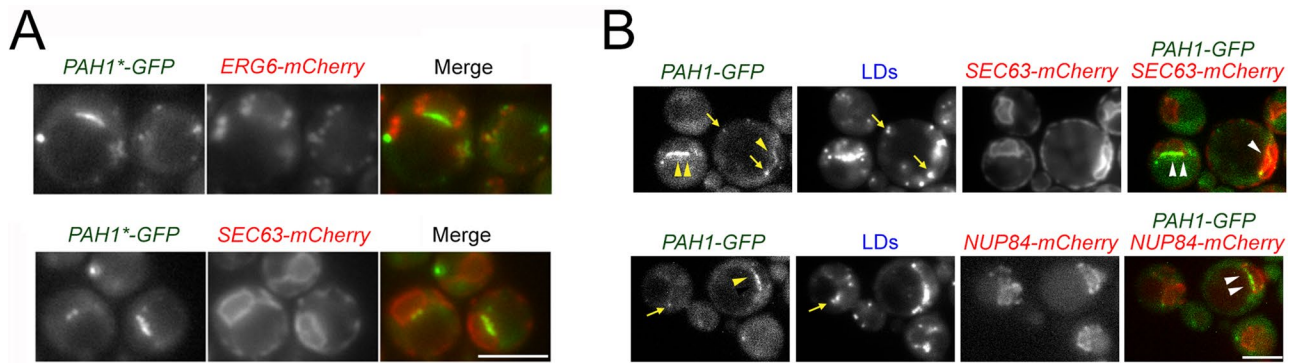
FIGURE 2: Pah1*-GFP and Pah1-GFP membrane targeting during glucose starvation. (A) Wild-type cells expressing the indicated fusion proteins and growing in the exponential phase were transferred to medium lacking glucose for 1 h and imaged with a Zeiss Axioplan epifluorescence microscope. (B) Top, pah1Δ cells expressing PAH1-GFP from a centromeric plasmid and SEC63-mCherry and growing in the exponential phase were transferred to medium lacking glucose for 30 min and imaged as in A. Cells were stained with MDH to label LDs. Bottom, wild-type cells expressing chromosomally integrated PAH1-GFP and NUP84-mCherry were subjected to glucose starvation as described. Arrows point to Pah1-GFP puncta in the proximity of LDs; arrowheads point to Pah1-GFP associated with the NVJ. Scale bar, 5 μm.

Because Pah1*-GFP targets the nuclear membrane at the diauxic shift, we tested whether glucose regulates this translocation. Indeed, acute glucose starvation of exponentially growing cells targets Pah1*-GFP to the NVJ (40 ± 7%). In addition, in 24 ± 6% cells, Pah1*-GFP associates with punctuate structures, approximately half of which (44 ± 8%) are in contact with LDs (Figure 2A). Thus, in addition to LDs, Pah1*-GFP may associate with other organelles under these conditions. In many glucose-starved cells, Pah1*-GFP also targets the autophagosome (Supplemental Figure S5), suggesting a distinct role for Pah1 in macroautophagy, as recently shown for its mammalian orthologue, lipin-1 (Zhang et al., 2014). Of importance, after glucose starvation, wild-type Pah1-GFP expressed at endogenous levels showed a similar targeting as Pah1*-GFP (Figure 2B). Consistent with the increased instability of the catalytically active Pah1, fewer cells with membrane-bound Pah1-GFP could be detected (11 ± 7%), and their fluorescence signal was lower than that of Pah1*-GFP. As expected, no membrane-bound Pah1-GFP was detected in exponential phase (unpublished data). Thus wild-type Pah1-GFP behaves similarly to Pah1*-GFP in response to glucose depletion and targets the NVJ, LDs, and additional foci.

Metabolic activation of Nem1-Spo7 triggers Pah1*-GFP recruitment to the nuclear membrane

Next we investigated the mechanism of Pah1 translocation to the nuclear membrane in response to nutrient starvation and growth phase. Because phosphorylation inhibits Pah1 membrane binding (Karanasios et al., 2010; Choi et al., 2011) and Pho85-Pho80 and protein kinase A (PKA), which phosphorylate Pah1 (Choi et al., 2012; Su et al., 2012), are controlled by nutrients, we asked whether inactivation of these kinases could target Pah1 to the nuclear membrane in glucose-replete medium. In pho85Δ or in cells in which PKA activity was chemically inhibited, Pah1*-GFP remained soluble in the cytosol during exponential phase (Figure 3, A and C). Msn2-mCherry translocated into the nucleus under these conditions, confirming the loss of PKA activity upon chemical inhibition (Figure 3B). Similarly, Pah1*-GFP targeting was not compromised in the PDS phase (Figure 3C) in cells lacking SNF1, which encodes the yeast AMP-activated serine/threonine protein kinase and plays a major role in glucose derepression (de Virgilio, 2012). Therefore Pah1*-GFP targeting does not require the glucose repression machinery.

Because the inhibition of nutrient-activated kinases involved in Pah1 regulation fails to trigger its recruitment under progrowth conditions, we asked whether Pah1 dephosphorylation, which is catalyzed by the conserved Nem1-Spo7 complex (Santos-Rosa et al., 2005), could be the limiting step for recruitment. Of interest, Nem1-Spo7 exhibits optimal activity toward recombinant Pah1 at acidic pH, which is unusual for an ER enzyme with a cytosolic substrate (Su et al., 2014). Because a decrease in glucose levels is accompanied by acidification of the cytosol, reaching pH 5.0 at the PDS phase (Orij et al., 2012), we asked whether pH-dependent Pah1 dephosphorylation governs its targeting to the nuclear membrane at the PDS phase. The following data suggest that this is the case. First, endogenously phosphorylated Pah1 purified from Saccharomyces cerevisiae was more efficiently dephosphorylated in vitro by Nem1-Spo7 at pH 5.0, as indicated by the faster-migrating band corresponding to dephosphorylated Pah1 (Figure 4A; O'Hara et al., 2006). Second, Pah1*-GFP targeted the NVJ in pma1-007 cells—which exhibit decreased activity of the plasma membrane ATPase Pma1, the major regulator of cytosolic pH in yeast—but not in wild-type cells, grown in glucose-rich medium at pH 3.0 for 1 h (Figure 4, B and C). Similarly, Pah1*-GFP targeted NVJ in cells treated with 100 mM sodium acetate at pH 4.8 but not at pH 7.0 (Figure 4, D and E). Sodium acetate induces weak acid stress at pH values below or near 4.76, the pKa of acetate, since a significant amount is protonated and can diffuse into the cytosol (Mollapour et al., 2008). Third, if pH-dependent Nem1-Spo7 activation is the limiting step of Pah1 targeting, then overexpression of Nem1-Spo7 under nutrient-replete conditions should mimic the kinetics of Pah1 membrane recruitment during starvation. We recently showed that Nem1-Spo7 overexpression targets wild-type Pah1-GFP to LDs (Karanasios et al., 2013) but did not investigate early events of this recruitment. Strikingly, after 2 h of growth in galactose media, 47 ± 7% of GAL-NEM1/SPO7 cells show clear targeting of Pah1-GFP to the NVJ. As the induction persisted, NVJ localization gradually decreased, with many cells showing discontinuous NVJ targeting and concomitant LD enrichment at 3 h of induction (Figure 5, A and B), suggesting that Pah1 moves from NVJ onto LDs.

Deletion of the C-terminal tail of Pah1*-GFP, which is required for interaction with Nem1-Spo7 (Karanasios et al., 2013), prevented targeting onto membranes during glucose starvation or the PDS phase
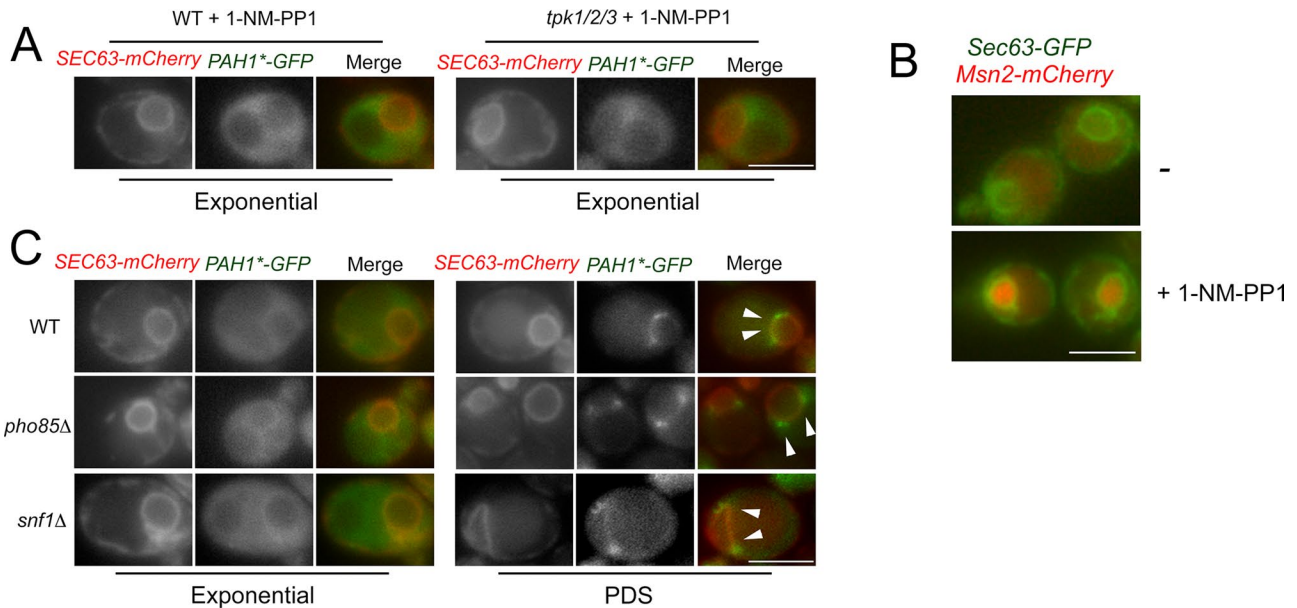
FIGURE 3: Role of Pho85, PKA, or Snf1 in the targeting of Pah1 to the nuclear envelope and LDs during the PDS phase. (A) Wild-type (WT) cells (W303) or PKA-deficient cells carrying mutations in the ATP-binding pockets of the three catalytic subunits of PKA ($TPK1^{M164G}$ $TPK2^{M147G}$ $TPK3^{M165G}$; $tpk1/2/3$) that make them sensitive to 1-NM-PP1 were transformed with the indicated reporter constructs. 1-NM-PP1 is a cell-permeable ATP-analogue that inhibits only the modified Tpk subunits (Yorimitsu et al., 2007). Cells in early exponential phase were treated with 5 µM 1-NM-PP1 for 5 min at 30°C min and immediately mounted for observation. No change in distribution of Pah1*-GFP was observed. (B) $tpk1/2/3$ cells expressing the indicated reporters were treated with or without 1-NM-PP1 as in A. (C) Wild-type, $pho85\Delta$ or $snf1\Delta$ deletion mutants expressing the indicated reporters were grown in exponential or PDS phase as described in Figure 1, B and C, and imaged by epifluorescence microscopy. Scale bar, 5 µm.

(Supplemental Figure S6). Under either of these growth conditions, Nem1-GFP localizes to a punctum in wild-type cells, similar to what was described for Nem1 during exponential phase (Adeyo et al., 2011), but also displayed a nuclear membrane distribution (Supplemental Figure S7).

The requirement of Nem1-Spo7 for Pah1 activation can be bypassed by mutating seven Pah1 phosphorylated residues to alanines (7A mutant; O'Hara et al., 2006; Karanasios et al., 2010; Choi et al., 2011). Consistently, Pah1*-7A-GFP targets the NVJ even in glucose-replete media (Figure 5C). Of importance, this mutant still translocates to perinuclear LDs during the PDS phase (Figure 5C). Therefore increased TAG levels correlate with the concentration of Pah1*-7A-GFP in contact with LDs. Collectively our results show that Nem1-Spo7 activation drives Pah1 to the NVJ, and this precedes Pah1 localization to LDs for TAG production.

Because constitutive membrane binding of Pah1*-7A-GFP does not cause a major growth defect in glucose-replete media, PA must be still available for lipid synthesis and/or the endogenous Pah1 must compete with the catalytically dead enzyme. However, overexpression of Pah1*-7A, but not Pah1*, causes slow growth, defects in lipid droplet biogenesis, derepression of *INO1* transcription, and nuclear/ER membrane expansion (Figure 5, D–G). These phenotypes are all observed in $pah1\Delta$ cells, suggesting that excess Pah1*-7A has a dominant-negative effect by blocking the access of endogenous Pah1 to PA. Indeed, co-overexpression of wild-type Pah1 rescued the slow growth of Pah1*-7A (Figure 5D), which indicates that these enzymes compete for binding to a common pool of PA at the nuclear membrane.

ER membrane organization is defective in cells lacking LDs in the PDS phase

We next asked whether LD formation at the nuclear membrane is required for the targeting of Pah1*-GFP. Production of neutral lipids, and concomitant biogenesis of LDs, is absent in cells lacking the steryl acyltransferases *ARE1* and *ARE2* and the DAG acyltransferases *DGA1* and *LRO1* (Oelkers et al., 2002; Petschnigg et al., 2009). Pah1*-GFP still targets the nuclear envelope in cells lacking the four acyltransferases (hereafter called 4Δ) at the PDS phase (Figure 6A) and colocalizes with Nem1-tdTomato (Figure 6, B and C). Association of Pah1*-GFP with Nvj1-mCherry was seen in 26 ± 7% of the cells under these conditions. Of interest, we observed membrane proliferation in 4Δ cells when Pah1*-GFP targets the nuclear envelope, as visualized by the Sec63 reporter. Both nuclear and peripheral ER membrane organization is affected, leading to severe defects in nuclear shape and cortical ER organization (Figure 7A). These defects are seen in the $dga1\Delta lro1\Delta$ double mutant but not in $are1\Delta are2\Delta$ in the PDS phase (Figure 7A) and are absent in 4Δ cells in the exponential phase (Petschnigg et al., 2009; see Figure 9C later in the article). Thus membrane proliferation is observed only upon Pah1 activation and under conditions that block acylation of DAG. Altered membrane morphology is not due to increased lethality of the 4Δ strain, as cells with nuclear/ER defects do not stain with propidium iodide, even 24 h after the PDS time at which relative viability is similar to that of the wild-type strain (Supplemental Figure S8). These membrane changes were accompanied by significant increases in DAG, ergosterol, fatty acids, and total phospholipids, including phosphatidylinositol, phosphatidylserine, phosphatidylethanolamine, and phosphatidylcholine (PC; Figure 7, B and C).
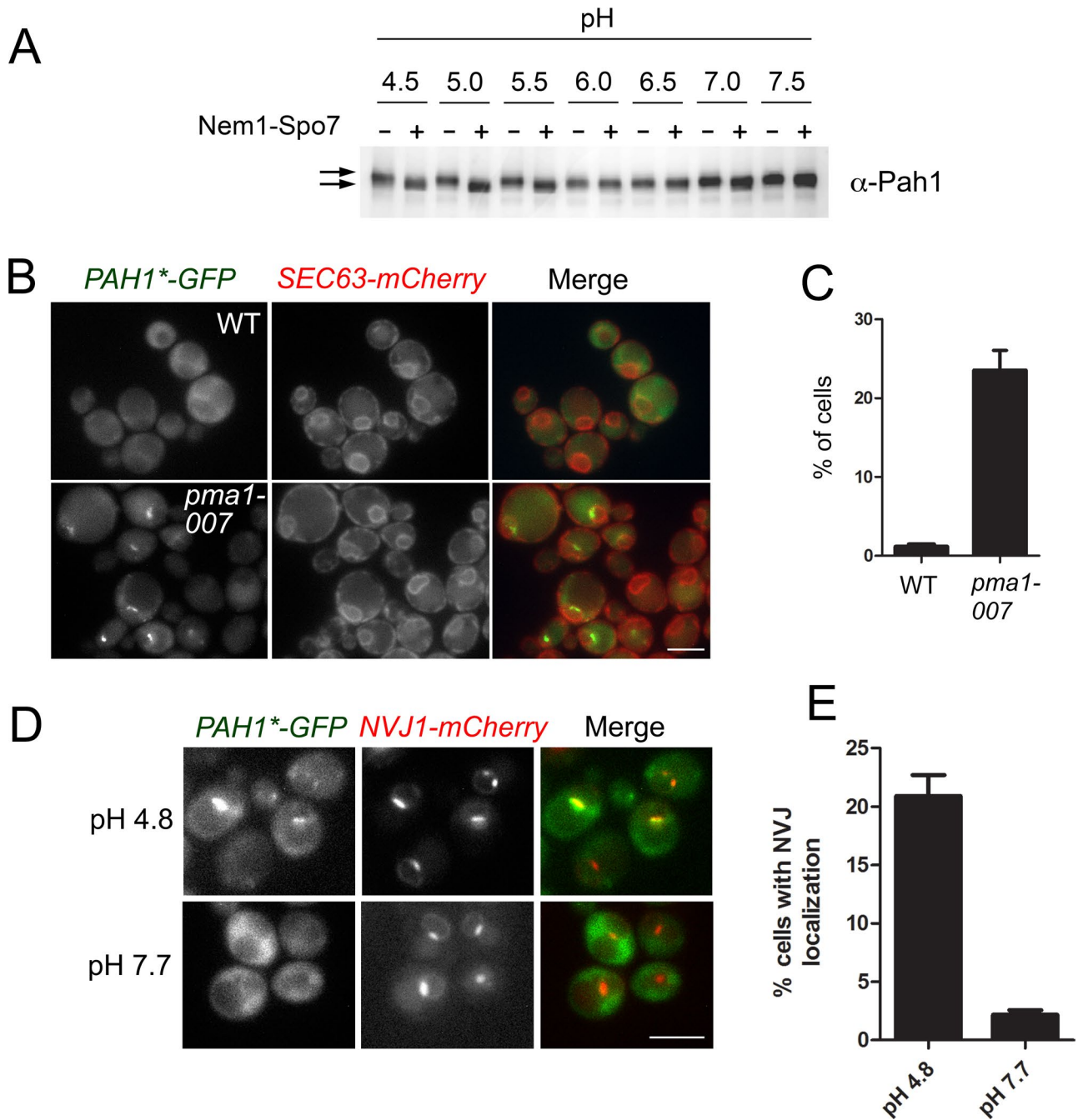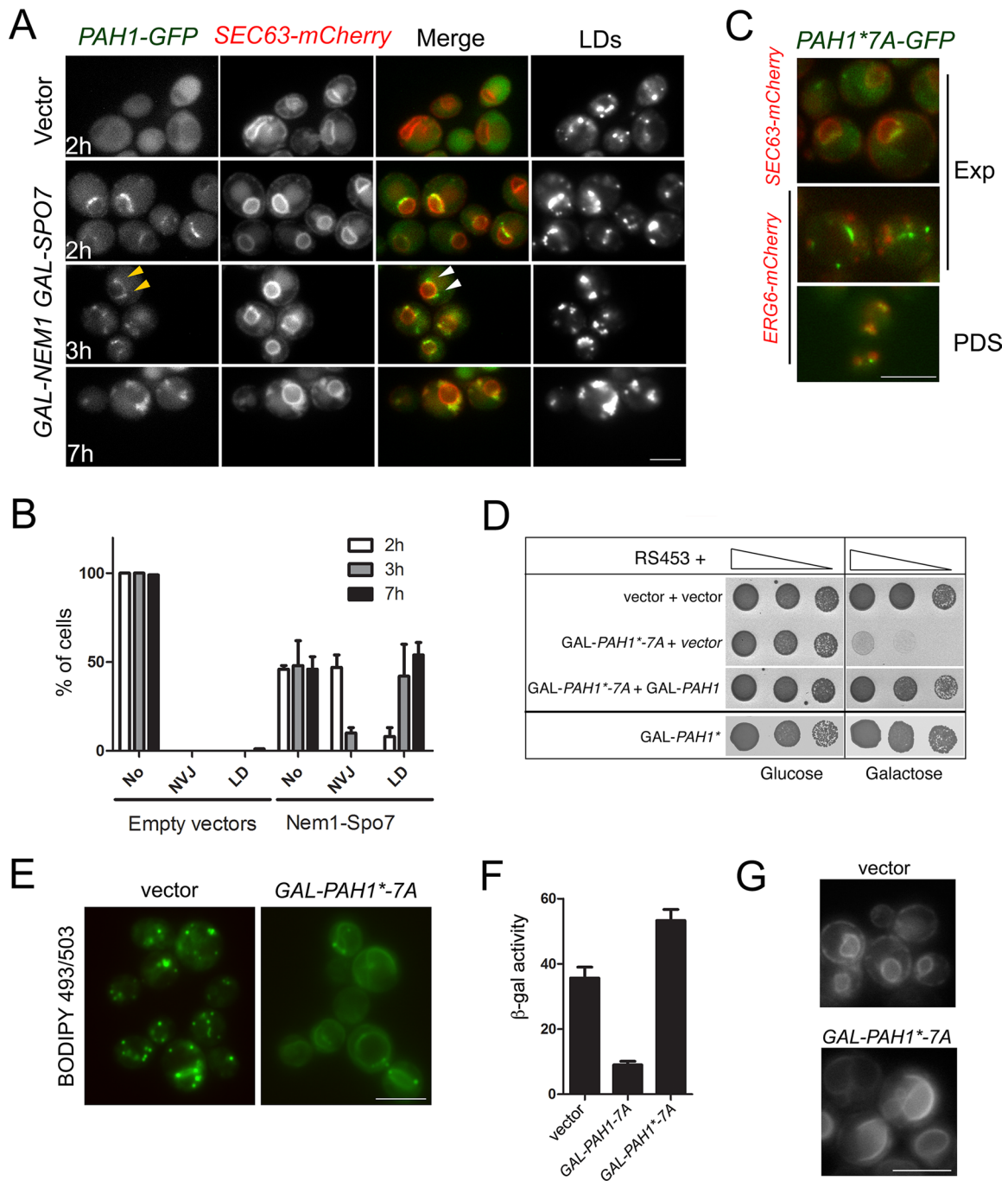
FIGURE 4: Metabolic regulation of Nem1-Spo7 controls Pah1 targeting to the nuclear envelope. (A) pH-dependent dephosphorylation of Pah1 by the Nem1-Spo7 complex. In vitro reactions using purified proteins at the indicated pH were performed as described in *Materials and Methods*. Arrows point to the different Pah1 electrophoretic mobilities. (B) Wild-type or *pma1-007* cells expressing the indicated fusion proteins were transferred to medium at pH 3.0, grown for 1 h and imaged as in Figure 1C. (C) Quantification of the Pah1*-GFP targeting to the nuclear envelope shown in B. Two hundred cells from two independent experiments were scored. (D) Pah1*-GFP targets the NVJ in media buffered to pH 4.8. Wild-type cells (RS453) expressing chromosomally integrated Nvj1-mCherry and Pah1*-GFP were grown to the exponential phase and resuspended in SC medium 2% glucose with 100 mM sodium acetate buffered at pH 4.8 or 7.7, respectively, for 1 h at 30°C before imaging. (E) Quantification of the Pah1*-GFP targeting in the sodium acetate media shown in Figure 4D. One hundred cells from two independent experiments were scored. Scale bar, 5 µm (B, D).

Lipid metabolism and ER membrane organization are rewired in cells lacking LDs

Our data suggest that Pah1 targeting to the nuclear envelope acts as a metabolic switch to divert PA from phospholipids into TAG stored in LDs. In the absence of TAG storage, DAG could be used for phospholipid synthesis and membrane biogenesis, either by the Kennedy pathway or by Dgk1-dependent synthesis of PA (Figure 8A). The rate-limiting step in the Kennedy pathway of PC synthesis is catalyzed by the conserved cholinephosphate cytidylyltransferase Pct1. Deletion of either *DGK1* or, to a lesser degree, *PCT1* restored

FIGURE 5: Dephosphorylation bypasses the metabolic regulation of Pah1 targeting to the nuclear envelope. (A) Sequential targeting of Pah1-GFP to the NVJ and LDs induced by increasing Nem1-Spo7 levels. *pah1Δ* cells expressing the indicated fusion proteins and carrying the *GAL-NEM1* and *GAL-SPO7* plasmids or the corresponding empty vectors were transferred to galactose-containing medium for 2, 3, and 7 h and imaged as described. Arrowheads point to cells where the LD-associated pools of Pah1 are linked with a thin nuclear membrane thread. (B) Quantification of the Pah1-GFP targeting shown in A. Two hundred cells from two independent experiments were scored. (C) Dephosphorylation of Pah1*-GFP targets the nuclear envelope constitutively in glucose media. Wild-type cells expressing the indicated fusion proteins were imaged in the exponential or PDS phase, respectively, with a Zeiss Axioplan epifluorescence microscope. (D) Overproduction of the catalytically inactive and constitutively nuclear membrane-bound Pah1*-7A is dominant negative. Serial dilutions of wild-type cells carrying an empty vector or the indicated GAL-inducible *PAH1* constructs were spotted onto synthetic plates supplemented with either glucose (left) or galactose (right) and grown for 1.5 or 3 d, respectively, at 30°C. (E) Wild-type cells expressing the indicated plasmids were labeled with BODIPY 493/503 to visualize LDs. Overexpression of Pah1*-7A causes a significant decrease in LD number and the appearance of BODIPY-enriched membranes, similar to those described for *pah1Δ* (Adeyo *et al.*, 2011). (F) Cells carrying an *INO1* promoter-lacZ reporter were assayed for β-galactosidase activity as described in *Materials and Methods*. (G) Cells expressing *SEC63-GFP* to depict nuclear/ER membrane morphology were visualized by epifluorescence microscopy. Scale bar, 5 μm (A, C, E, G).
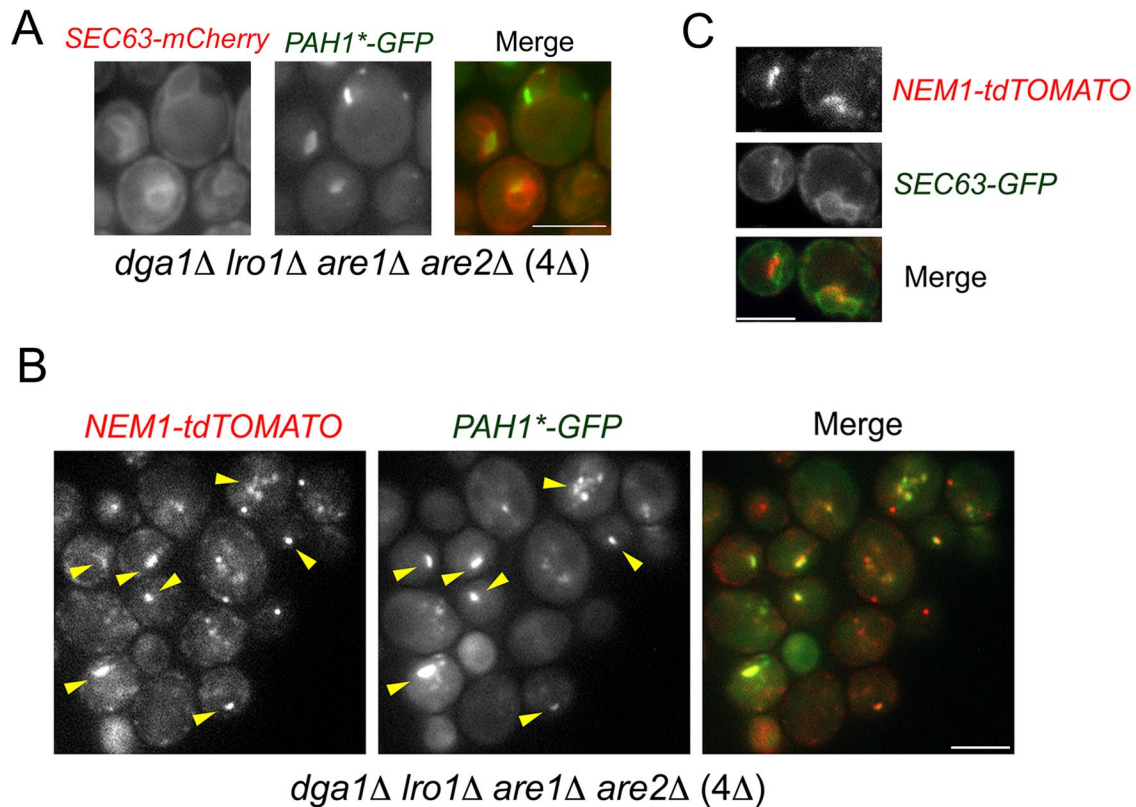
FIGURE 6: Membrane targeting of Pah1*-GFP in the absence of LDs. (A) The quadruple acyltransferase mutant (4Δ) expressing the indicated fusion proteins was grown to the PDS phase and imaged live. (B) Colocalization of Nem1-tdTomato and Pah1*-GFP in 4Δ cells. Cells were grown to the PDS phase and imaged as in A. (C) Nem1-tdTomato localizes on the nuclear membrane in 4Δ cells at the PDS phase. Scale bar, 5 µm.

partially nuclear morphology in 4Δ cells, as visualized by Sec63-GFP, although we noticed that cytoplasmic membrane build-up is still present in 4Δ dgk1Δ cells (Figure 8B). To investigate in more detail how lipid metabolism is rewired in the PDS phase in the 4Δ mutant and whether this affects membrane organization, we examined ER membrane morphology at the ultrastructural level in 4Δ, 4Δ pct1Δ, and 4Δ dgk1Δ mutants. Consistent with the fluorescence data, electron microscopy revealed that ER membrane proliferation in 4Δ cells, which was more evident in the ER subpopulation connecting the nucleus with the plasma membrane–associated cortical ER ("cytoplasmic ER"; Figure 8, C and D). This was decreased modestly by deletion of PCT1. Deletion of DGK1 rescued both cytoplasmic and cortical ER expansion almost back to wild-type levels (Figure 8, C and D). We noticed that the ER morphology is reorganized in this mutant, with a striking appearance of cytoplasmic ER agglomerates (Figure 8, C and D). We also noticed fragmented ER and giant mitochondria in $17 \pm 4\%$ and $18 \pm 5\%$ of 4Δ dgk1Δ cells, respectively. Of importance, DAG levels increased significantly in 4Δ dgk1Δ compared with 4Δ, suggesting that Dgk1 is indeed active in converting DAG to PA in the 4Δ cells (Figure 8E). However, total phospholipids showed, surprisingly, a further increase in 4Δ dgk1Δ when compared with the 4Δ cells. This suggests that another phospholipid biosynthetic pathway is up-regulated in the 4Δ dgk1Δ cells to detoxify DAG and could be responsible for the accumulation of the ER agglomerates seen in this mutant. Therefore we blocked the PC branch of the Kennedy pathway by generating a 4Δ dgk1Δ pct1Δ sextuple mutant complemented with a URA3-based DGK1 plasmid and

monitored the ability of cells to recover after the PDS phase in the absence of DGK1. As seen in Figure 8F, deletion of PCT1 in the 4Δ dgk1Δ mutant results in potent growth inhibition. Therefore, in the absence of TAG synthesis, both Dgk1- and Pct1-dependent pathways are required for membrane homeostasis and viability.

Regulation of Pct1 targeting to the nuclear membrane by growth phase

Pct1 is a soluble enzyme that is activated upon membrane binding (Cornell and Northwood, 2000) and in yeast interacts with the karyopherin Kap60, which mediates nuclear import (MacKinnon et al., 2009). Of interest, in exponentially growing wild-type cells, Pct1 is found exclusively on the nuclear membrane, but in the PDS phase, it is released from membranes and localizes into the nucleus (Figure 9, A and C). Release of Pct1 from the nuclear membrane takes place at the diauxic shift, coinciding with the recruitment of Pah1 (Figure 9A); it is also induced by glucose starvation, indicating that it is regulated by nutrient signals in a manner opposite to that of Pah1 (Figure 9B). Of importance, Pct1 remained bound to the nuclear membrane of 4Δ cells in the PDS phase, when nuclear shape was deformed (Figure 9, C and D). Expression of Dga1, which acylates DAG, restored LD formation, nuclear shape, and the concomitant release of Pct1 from the nuclear membrane into the nucleus in 4Δ (Figure 9E). Thus, channeling DAG to LDs at the nuclear envelope regulates membrane biogenesis. Overexpression of Nem1-Spo7, which targets Pah1 to the nuclear membrane and results in LD formation, also led to an increase in the intranuclear pool

A
SEC63-GFP / PUS1-RFP

wild-type 4Δ

dga1Δ lro1Δ are1Δ are2Δ

B

C
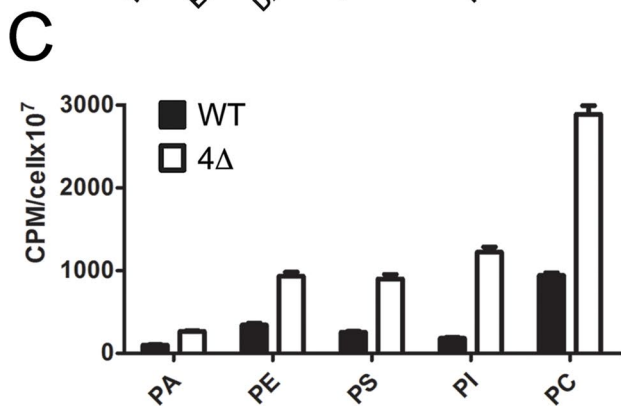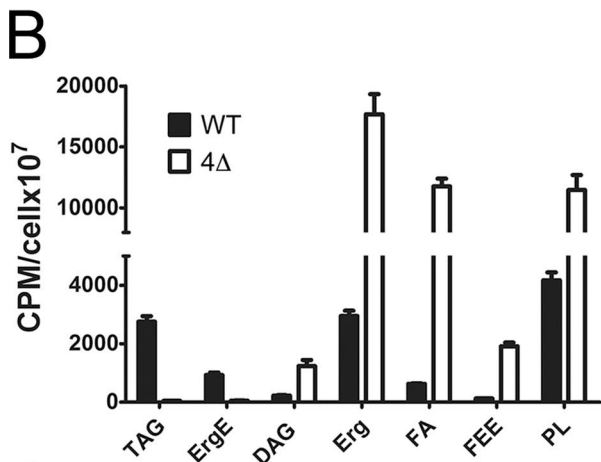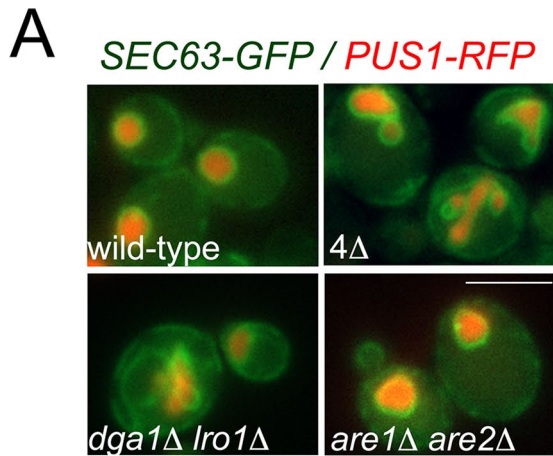
FIGURE 7: Nuclear/ER membrane defects and lipid composition of cells lacking LDs in the PDS phase. (A) Nuclear shape and ER membrane organization in the indicated strains, visualized by an intranuclear (*PUS1-RFP*) or ER reporter (*SEC63-GFP*), respectively. Images were acquired with a Zeiss Axioplan epifluorescence microscope. Scale bar, 5 μm. (B) Neutral lipid composition of the wild-type (BY4742) and the 4Δ strains in the PDS phase. Cells were labeled and lipids were extracted and separated as described in *Materials and Methods*. Each data point represents the mean ± SD of three experiments. Erg, ergosterol; ErgE, ergosterol ester; FA, fatty acid; FEE, fatty ethyl ester; PL, phospholipid; TAG, triacylglycerol. (C) Phospholipid composition of the wild-type (BY4742) and the 4Δ strains in the PDS phase. Cells were labeled and lipids were extracted and separated as described in *Materials and Methods*. Each data point represents the mean ± SD of three experiments. PC, phosphatidylcholine; PE, phosphatidylethanolamine; PI, phosphatidylinositol; PS, phosphatidylserine.

of Pct1 (Supplemental Figure S9). Of interest, Pah1 and Pct1 are amphitropic proteins that are recruited to the nuclear membrane via amphipathic helices in a phosphorylation-dependent mechanism. Therefore reversible targeting of soluble enzymes may govern lipid homeostasis in response to changing growth conditions.

DISCUSSION
All cells must continuously balance the flux of lipid metabolites between membranes for growth or storage for survival during nutrient deprivation. Addressing the mechanisms of this regulation is critical for a better understanding of prevalent metabolic diseases such as diabetes or obesity, as well as of cancer, which is characterized by a high demand of lipid synthesis to support cell proliferation. The data presented here provide evidence that compartmentalized activity of Pah1 at the nuclear membrane acts as a switch that controls the balance between membrane and storage lipids.

Despite its central role in lipid metabolism, Pah1 shows a predominantly soluble distribution, reflecting its highly dynamic association with membranes. Addressing its regulation is further complicated by the fact that Pah1 is unstable when activated by Nem1-Spo7 dephosphorylation due to proteasomal degradation (Hsieh et al., 2015). To overcome these problems, we used a catalytically dead Pah1 mutant (Pah1*) that is partially stabilized (Pascual et al., 2014) and can be detected on membranes (Karanasios et al., 2010). Although we cannot exclude that interfering with Pah1 stability might affect its localization, the fact that wild-type Pah1 responds to both glucose starvation and Nem1-Spo7 overexpression by targeting the same compartments as Pah1* suggests that the latter is a physiologically relevant reporter for the localization of Pah1. In addition, wild-type mouse lipin2 also targets LDs during the PDS phase, indicating that at least some aspects of this nutrient-dependent regulation are evolutionarily conserved.

When yeast cells exit exponential growth, they accumulate TAG, which can be used for survival during lengthy starvation periods (Kohlwein et al., 2013). Under these conditions, Pah1 targets a punctum on the nuclear membrane that contacts LDs. Of interest, at the same time point, the DAG acyltransferase Dga1 localizes on the LD surface. Therefore, if Pah1-generated DAG at the nuclear membrane is acylated to form TAG, some channeling event is likely to be required to transfer DAG to the growing LD. It is possible that a pool of Pah1 is also present on LDs but not readily detectable by our imaging conditions, although a recent high-confidence proteomic analysis did not identify Pah1 within the LD protein inventory (Currie et al., 2014). Alternatively, DAG in close proximity to the forming LD might perform a structural role during the emergence or expansion of LDs from the phospholipid bilayer, as proposed previously (Adeyo et al., 2011).

Remarkably, Pah1 and associated LDs concentrate at the nuclear envelope flanking the NVJ. It is conceivable that such an arrangement facilitates the passage of LDs to the vacuole through the NVJ contacts at later stages of the stationary phase, when LDs are degraded by lipophagy (Wang et al., 2014). Because Pah1 targets initially the NVJ at the diauxic shift, it is possible that the same enzyme pool concentrates subsequently to the flanking LD-associated sites. However, because Pah1 still localizes to a punctum at the nuclear membrane in *nvj1Δ* and TAG levels do not decrease in these cells, nuclear–vacuole contacts are not required for the targeting and function of Pah1 in TAG synthesis. Thus Pah1 may perform a distinct role at the NVJ. The NVJ mediates the microautophagic degradation of the nuclear membrane (PMN), which, similar to LD biogenesis, is induced by nutrient depletion and gradually builds up as cells exit the exponential phase. Other lipid metabolic enzymes
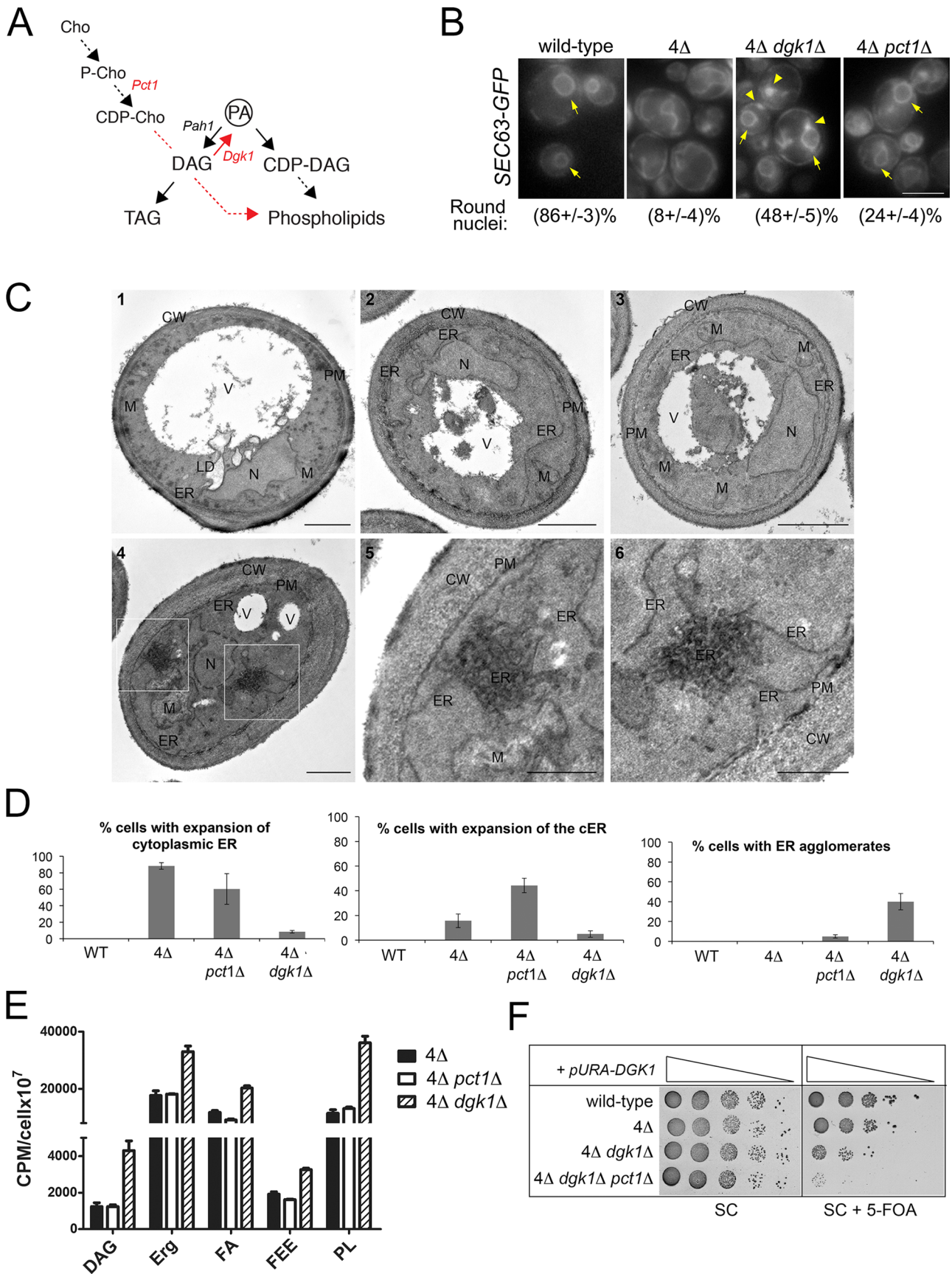
FIGURE 8: Role of phospholipid biosynthetic pathways in ER membrane remodeling in cells lacking LDs. (A) Schematic of the roles of Pct1 and Dgk1 in phospholipid synthesis. (B) Nuclear shape defects in the 4Δ mutant are partially rescued by deletion of *DGK1* or *PCT1*. The indicated strains expressing a *SEC63-GFP* were imaged at the PDS phase with a

also concentrate to the NVJ and are required for PMN (Kohlwein et al., 2001; Levine and Munro, 2001; Kvam and Goldfarb, 2007). Pah1 might thus temporarily coordinate PMN with LD biogenesis, two pathways of membrane lipid recycling that are induced by starvation. Alternatively, Pah1 might control another lipid transport step between the vacuole and the ER that needs to be coordinated with storage in LDs. Because the vacuole contains significant amount of lipids, their export through the NVJ and subsequent storage to the adjacent LDs could require Pah1, although this remains a speculation.

According to the electrostatic/hydrogen bond-switch mechanism, the ionization state of the PA head group is critical for its interaction with effector proteins (Kooijman et al., 2007). Factors like intracellular pH or local membrane environment can influence the charge of PA and thus its ability to interact with soluble proteins. Recent work suggests that mammalian lipins bind PA in vitro by the electrostatic hydrogen bond switch mechanism (Eaton et al., 2013, 2014). Cytosolic acidification, which takes place during starvation in yeast, will cause protonation of the PA head group and decreased interaction with PA-binding proteins (Shin and Loewen, 2011). However, Pah1 targets membranes and LDs in response to acidification (Figure 4) and starvation (Figures 1 and 2) in vivo and is required for TAG synthesis in stationary phase (Han et al., 2006). That the NVJ and LD targeting of Pah1 during starvation requires binding to Nem1-Spo7 (Supplemental Figure S6) and Nem1-Spo7 activity in vitro has a pH optimum of 5.0 (Su et al., 2014; Figure 4A) suggests that Nem1-Spo7 is critical for the growth phase-dependent activation of Pah1, although under these conditions, its PA substrate is protonated. Of interest, Nem1-Spo7 is regulated by TOR (Dubots et al., 2014), and a recent study demonstrated that glucose starvation–dependent TOR activation is governed by cytosolic acidification (Dechant et al., 2014), suggesting a possible link between growth-dependent pH and Nem1-Spo7 activity. Alternatively, acidification might also control Nem1-Spo7 function more directly. Future work will be needed to address these mechanisms.

Our data suggest that Dgk1 is active in 4Δ cells, converting DAG to PA, which could then be rerouted toward phospholipids and membrane biogenesis. Indeed, a role for Dgk1 in PA-mediated phospholipid synthesis has been described (Fakas et al., 2011). The facts that in the 4Δ dgk1Δ mutant, 1) phospholipids further increased compared with 4Δ, 2) cytoplasmic ER membrane agglomerates accumulated, and 3) ER membrane proliferation and nuclear shape defects were rescued point to a specific role of Dgk1 in channeling PA-derived phospholipids to the nuclear/ER membrane. Consistent with this, overexpression of Dgk1 activity leads to nuclear/ER membrane expansion (Han et al., 2008). In the absence of Dgk1, the Kennedy pathway might channel high DAG levels toward phospholipids. Previous work supports the notion that DAG produced by Pah1 can be redirected toward phospholipids via the Kennedy pathway: overexpression of a constitutively active Pah1 is toxic to cells but can be partially rescued by the supplementation of choline (Choi et al., 2011). The function of Dgk1 and Pct1 in maintaining DAG homeostasis is underscored by the strong growth inhibition of the 4Δ dgk1Δ pct1Δ mutant.

Loss of Pah1 and Nem1-Spo7 results in nuclear structure defects, characterized by a striking expansion of the nuclear and the ER membrane (Siniossoglou et al., 1998; Santos-Rosa et al., 2005). In spo7Δ cells, and presumably pah1Δ, this expansion takes place at the membrane adjacent to the nucleolus (Campbell et al., 2006). The nucleolus is frequently, although not always, associated with the nuclear membrane in contact with the vacuole (Kvam and Goldfarb, 2007). The special properties of this domain, characterized as a "membrane sink" (Witkin et al., 2012), could be due to the localized partitioning of glycerol backbones and fatty acids from membrane phospholipids to TAG in the nuclear envelope–associated LDs. Although the source of fatty acids that acylate DAG during nutrient depletion is unknown, phospholipid deacylation would be a prime candidate. Of interest, Lro1, which catalyzes the direct transfer of fatty acids from phospholipids to DAG, also relocalizes to a specific nuclear envelope domain during the PDS phase (Wang et al., 2012). We hypothesize that such interconversion not only might contribute to metabolic homeostasis during growth, also but might also be used for the control of nuclear structure when membrane needs to be added or removed from the nuclear envelope. Because the ER network is in contact with virtually most organelles, it is tempting to speculate that the positioning of LDs, which in yeast remain associated with the ER throughout their life cycle, may be relevant for local membrane- and organelle-remodeling events.

MATERIALS AND METHODS
### Yeast strains and plasmids
Yeast strains are listed in Table 1. Gene deletions and epitope tagging by chromosomal integration were generated by a one-step PCR-based method (Longtine et al., 1998; Janke et al., 2004) and confirmed by PCR. Plasmids are listed in Table 2.

Media and growth conditions
Unless stated otherwise, all reagents were purchased from Sigma (St. Louis, MO). Cells were transformed using the lithium acetate method. Yeast cells were grown in synthetic medium (SC) containing 2% glucose, 0.2% yeast nitrogen base (Difco, BD, Franklin Lakes, NJ), 0.6% ammonium sulfate, and amino acid drop-out (60 mg/l leucine, 55 mg/l adenine, 55 mg/l uracil, 55 mg/l tyrosine, 20 mg/l arginine, 10 mg/l histidine, 60 mg/l isoleucine, 40 mg/l lysine,

---

Zeiss Axioplan epifluorescence microscope. Arrows point to round nuclei; arrowheads point to bright, Sec63-GFP–positive spots in the cytoplasm. Percentage of cells with round nuclei. At least 200 cells/strain from two independent experiments were scored. Bar, 5 μm. (C) Electron microscopy analyses. Wild-type (1), 4Δ (2), 4Δ pct1Δ (3), and 4Δ dgk1Δ (4) cells were grown to the PDS phase before processing for electron microscopy. White squares in 4 delimitate the insets that contain typical examples of ER agglomerates and are shown in 5 and 6 at higher magnification. CW, cell wall; ER, endoplasmic reticulum; LD, lipid droplet; M, mitochondrion; N, nucleus; PM, plasma membrane; V, vacuole. Scale bar, 1 μm; inset, 500 nm. (D) Quantification of the ER membrane expansion shown in C was performed as described in *Materials and Methods*. (E) Neutral lipid composition of the indicated strains in the PDS phase. Cells were labeled and lipids were extracted and separated as described in *Materials and Methods*. Each data point represents mean ± SD of three experiments. Erg, ergosterol; FA, fatty acid; FEE, fatty ethyl ester; PL, phospholipid. (F) Loss of *PCT1* and *DGK1* in the 4Δ strain inhibits growth. The indicated strains expressing a pURA-*DGK1* plasmid were grown to the PDS phase before spotted on complete synthetic plates (SC) without or with 5-fluoroorotic acid (5-FOA). Cells were grown for 2 or 3 d, respectively, at 30°C.
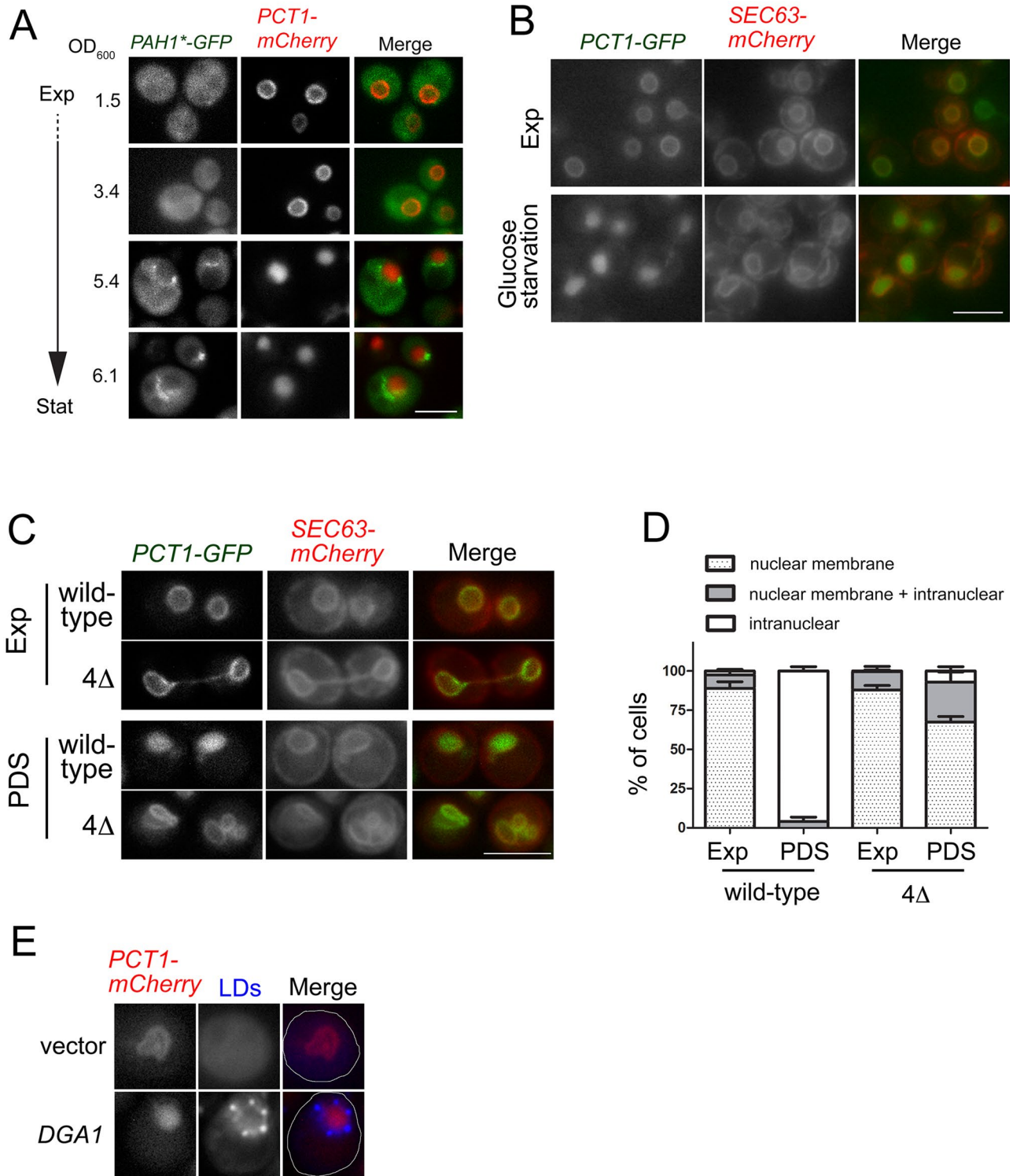
FIGURE 9: Membrane targeting of Pct1 is regulated in a growth- and nutrient-dependent manner. (A) Wild-type cells (BY4742) expressing chromosomally integrated *PCT1-Cherry* and Pah1*-GFP were grown to the indicated densities and imaged as in Figure 1C. (B) Wild-type cells (BY4742) expressing a chromosomally integrated *PCT1-GFP* and *SEC63-mCherry* growing in the exponential phase were transferred to medium lacking glucose for 30 min and imaged by epifluorescence microscopy, using a Zeiss Axioplan microscope. (C) Pct1-GFP localization in the presence or absence of LDs at the indicated growth phases. (D) Quantification of the Pct1-GFP relocalization shown in Figure 7C in wild-type and 4Δ cells. Two hundred cells per strain and condition from three independent experiments were scored. (E) DAG channeling to LDs restores nuclear shape in 4Δ cells. The 4Δ mutant expressing the indicated plasmids and *PCT1-mCherry* were grown to the PDS phase, and LDs were visualized using MDH labeling. The outlines of cells are shown in the merged images. Scale bar, 5 μm (A–C, E).

Strain	Genotype	Source/reference
RS453	MATα ade2-1 his3-11,15 ura3-52 leu2-3112 trp1-1	Wimmer et al. (1992)
SS2012	RS453 URA3::SEC63-mCherry	This study
SS2289	RS453 nvj1::HIS3MX6	This study
SS2110	RS453 nvj1::KanMX URA3::SEC63-mCherry	This study
SS1991	RS453 pah1::TRP1 NUP84-mCherry::KanMX	This study
SS2017	RS453 pah1::TRP1 ERG6-mCherry::KanMX	This study
SS1960	RS453 nem1::HIS3	Siniossoglou et al. (1998)
SS1744	RS453 ERG6-mCherry::KanMX	This study
SS1387	RS453 PAH1-GFP::KanMX	This study
SS2435	SS2012 brp1::KanMX (aka pma1-007)	This study
SS2502	RS453 NEM1-tdTOMATO::hphNT1	This study
SS2431	RS453 VPH1-mCherry::KanMX	This study
SS2512	RSY3077 NEM1-tdTOMATO::hphNT1	This study
SS2014	RS453 URA3:: NVJ1-mCherry	This study
BY4742	MATα his3Δ1 leu2Δ0 lys2Δ0 ura3Δ0	Open Biosystems
RSY3077	MATα his3Δ1 leu2Δ0 lys2Δ0 ura3Δ0 met15Δ0 are1::KanMX are2:KanMX trp1::URA lro1::TRP dga1::Lox-HIS-Lox	Jacquier et al. (2011)
RSY3018	MATα his3Δ1 leu2Δ0 lys2Δ0 ura3Δ0 met15Δ0 are1::KanMX are2:KanMX trp1::URA3	Roger Schneiter (University of Fribourg)
RSY3290	MATα his3Δ1 leu2Δ0 lys2Δ0 ura3Δ0 lro1::KanMX dga1::lox-HIS-lox	Roger Schneiter (University of Fribourg)
SS2437	RSY3077 pct1::HIS3MX6	This study
SS2468	RSY3077 dgk1::HIS3MX6	This study
SS2531	SS2468 pct1::NatMX6 YCplac33-DGK1	This study
SS2453	BY4742 PCT1-GFP::HIS3MX6	This study
SS2455	RSY3077 PCT1-GFP::HIS3MX6	This study
SS2449	BY4742 PCT1-mCherry::HIS3MX6	This study
SS2452	RSY3077 PCT1-mCherry::HIS3MX6	This study
W303-1B	MATα leu2-3112 ura3-1 his3-11,15 trp1-1 ade2-1 can1-100	Thomas and Rothstein (1989)
Y3527	W303-1B tpk1^{M164G}tpk2^{M147G}tpk3^{M165G}	Yorimitsu et al. (2007)
BY4741	MATa his3Δ0 leu2Δ0 met15Δ0 ura3Δ0	Open Biosystems
pho85Δ	BY4741 pho85::KanMX	Open Biosystems
snf1Δ	BY4741 snf1::KanMX	Open Biosystems

TABLE 1: Yeast strains used in this work.

60 mg/l phenylalanine, 50 mg/l threonine, 10 mg/l methionine, 40 mg/l tryptophan) lacking the appropriate amino acids for plasmid selection. For time-course growth experiments, cells were grown overnight at 30°C to the indicated optical densities. For GAL1/10 promoter–mediated overexpression, cells were initially pregrown in 2% glucose SC medium and then grown overnight in 2% raffinose SC medium, followed by transfer to SC medium containing 2% galactose to a final OD$_{600}$ of 0.2 and incubation at 30°C for the indicated times. For CUP1 promoter–mediated overexpression, cells were grown in copper-free medium (20 g/l glucose, 5 g/l ammonium sulfate, 1 g/l potassium phosphate, 0.5 g/l magnesium sulfate, 0.1 g/l sodium chloride, 0.1 g/l calcium chloride, 0.5 mg/l boric acid, 0.1 mg/l potassium iodide, 0.2 mg/l ferric chloride, 0.4 mg/l manganese sulfate, 0.2 mg/l sodium molybdate, 0.4 mg/l zinc sulfate,

2 µg/l biotin, 400 µg/l calcium pantothenate, 2 µg/l folic acid, 400 µg/l niacin, 200 µg/l p-aminobenzoic acid, 400 µg/l pyridoxine hydrochloride, 200 µg/l riboflavin, 400 µg/l thiamine hydrochloride, and amino acid drop-out lacking the appropriate amino acids for plasmid selection) and incubated with 0.5 mM CuSO$_4$ for the indicated times.

For growth assays on plates, yeast cells were grown in the corresponding SC liquid medium with the appropriate carbon source to early logarithmic phase. Ten microliters of serial 10-fold dilutions was spotted onto the appropriate SC plates and incubated at 30°C for 2–4 d. For PKA inactivation experiments, 5 µM C3-1'-naphthyl-methyl PP1 (1NM-PP1; Calbiochem Merck Millipore, Billerica, MA) was added to cells in exponential phase (OD$_{600}$ of ~0.5) and incubated at 30°C for the indicated times.

Plasmid	Description	Source/reference
YCplac111-*PAH1-D398A/D400A-GFP*	*PAH1-D398A/D400A-GFP* under control of *PAH1* promoter in *CEN/LEU2* vector	Karanasios *et al.* (2010)
pAS211-*GAL1/10-NEM1*	*NEM1* under control of *GAL1/10* promoter in *CEN/ADE2* vector	Karanasios *et al.* (2013)
pRS313-*GAL1/10-SPO7*	*SPO7* under control of *GAL1/10* promoter in *CEN/HIS3* vector	Karanasios *et al.* (2013)
YCplac111-*PAH1-D398A/D400A-7A-GFP*	*PAH1-D398A/D400A-7A-GFP* under control of *PAH1* promoter in *CEN/LEU2* vector	This study
YCplac33-*GAL1/10-PAH1-D398A/D400A-7A*	*PAH1-D398A/D400A-7A* under control of *GAL1/10* promoter in *CEN/URA3* vector	This study
YEplac181-*GAL1/10-PAH1*	*PAH1* under control of *GAL1/10* promoter in *2µ/LEU2* vector	O'Hara *et al.* (2006)
YEplac181-*GAL1/10-PAH1-D398A/D400A*	*PAH1-D398A/D400A* under control of *GAL1/10* promoter in *CEN/LEU2* vector	This study
YCplac33-*SEC63-mCherry*	*SEC63-mCherry* under control of *SEC63* promoter in *CEN/URA3* vector	This study
YCplac111-*SEC63-GFP*	*SEC63-GFP* under control of *SEC63* promoter in *CEN/LEU2* vector	Santos-Rosa *et al.* (2005)
pRS313-*PUS1-RFP*	*PUS1-RFP* under control of *PUS1* promoter in *CEN/HIS3* vector	Han *et al.* (2008)
YEplac111-*Lipin2-GFP*	*Lipin2-GFP* under control of *PAH1* promoter in *2µ/LEU2* vector	This study
pCumCheV5Atg8416	*ATG8*-mCherry under control of *CUP1* promoter in *CEN/URA3* plasmid	This study
YCplac33-*MSN2-mCherry*	*MSN2-mCherry* under control of *MSN2* promoter in *CEN/URA3* vector	This study
YCplac111-*PAH1-D398A/D400A-Δ837-GFP*	*PAH1-D398A/D400A-Δ837-GFP* under control of *PAH1* promoter into *CEN/LEU2* vector	This study
YCplac111-*NUP84-mCherry*	*NUP84-mCherry* under control of *NUP84* promoter in *CEN/LEU2* vector	This study
YCplac33-*DGA1-mCherry*	*DGA1-mCherry* under control of *DGA1* promoter in *CEN/URA3* vector	This study
YCplac22-pCup1-*NEM1*	*NEM1* under control of *CUP1* promoter in *CEN/TRP1* vector	This study
YCplac33-pCup1-*SPO7*	*SPO7* under control of *CUP1* promoter in *CEN/URA3* vector	This study
YCplac111-*NEM1-GFP*	*NEM1-GFP* under control of *NEM1* promoter in *CEN/LEU2* vector	This study
pUC-*NEM1-tdTomato*	*NEM1-tdTomato* hygromycin knock-in construct	Adeyo *et al.* (2011)

TABLE 2: Plasmids used in this work.

Fluorescence microscopy

Cells were grown at 30°C in synthetic medium, pelleted at the appropriate density, and immediately imaged live at room temperature. For imaging, we used two microscopes; for most experiments, we used a Zeiss AxioImager epifluorescence upright microscope with a 100× Plan-Apochromatic 1.4 numerical aperture (NA) objective lens (Carl Zeiss, Jena, Germany). Images were recorded using a large chip sCMOS mono camera for sensitive fluorescence imaging (ORCA Flash 4, version 2; Hamamatsu, Hamamatsu, Japan). Raw image files were saved by Zeiss ZEN blue software and exported to Photoshop (Adobe, San Jose, CA). Where indicated, images were acquired using a Zeiss Axioplan epifluorescence microscope and a 100× Plan-Apochromatic 1.4 NA objective lens connected to a Hamamatsu ORCA R2 charge-coupled device camera. Raw files were saved by Simple PCI6 software (Hamamatsu) and exported to Photoshop. For lipid droplet labeling, cells were stained for 10 min with 1.25 µg/ml BODIPY 493/503 (D-3922; Invitrogen, Carlsbad, CA) or 10 µM monodansylpentane (MDH; SM1000a; Abgent, San Diego, CA) at room temperature. For propidium iodide staining, cells were incubated with 20 µg/ml propidium iodide for 10 min in the dark.

All microscopy images were captured blindly. Quantification was performed on fields obtained from independent experiments. Quantification of Pct1-GFP localization was performed using ImageJ. A line across the nucleus was drawn, and pixel intensity was plotted for Pct1-GFP and Sec63-mCherry, using a 5-pixel average width. Cells were scored for intranuclear localization when mean *PCT1-GFP* pixel intensity increased between Sec63-mCherry maximal pixel intensities.

For three-dimensional (3D) analysis, through-focus image series were acquired on an AxioImagerZ2 fluorescence microscope (Zeiss) using Zen Blue 2012 software (Zeiss). Image series were subsequently deconvolved with Volocity 6.3 (PerkinElmer, Waltham, MA) using calculated point-spread functions and 3D iterative restoration processing to form 3D image stacks. Stacks were then visualized using Volocity to generate the 3D images.

Electron microscopy

For electron microscopy, cells were grown to the postdiauxic phase and processed as previously described (Griffith *et al.*, 2008). For statistically assessing the ER proliferation, the ER was divided into three major subdomains: the nuclear envelope, the cortical ER (the ER adjacent to the plasma membrane), and the cytoplasmic ER

(the ER connecting the nuclear envelope with the cortical ER). Three different grids with sections obtained from the same preparations were evaluated. For every grid, the percentage of cells displaying ER proliferation in one of the three subdomains was determined by examining 100 randomly selected cell profiles. We analyzed 300 cells/strain.

Cytosol acidification and glucose starvation

pma1-007 and the corresponding wild-type strain were grown in SC medium containing 2% glucose and buffered with 50 mM sodium phosphate, pH 7.0, to exponential phase (OD_{600} of ~0.5), pelleted, and resuspended into SC medium 2% glucose, pH 3.0 (adjusted with HCl), and incubated at 30°C for 1 h. Cells treated with acetate were first grown in SC medium 2% glucose to exponential phase, pelleted, resuspended into SC medium 2% glucose containing 100 mM sodium acetate buffered to pH 4.8 or 7.7, and incubated at 30°C for 1 h. For glucose starvation experiments, cells in exponential phase were washed once with SC medium lacking carbon source, resuspended in the same volume of SC medium lacking carbon source, and incubated at 30°C for the indicated times.

Nem1-Spo7 phosphatase assay

All steps of enzyme purification were performed at 4°C. The protein A–tagged Nem1-Spo7 complex was purified by immunoglobulin G (IgG)–Sepharose affinity chromatography as previously described (Siniossoglou *et al.*, 2000), with minor modifications. Briefly, the cell extract was prepared by lysis with glass beads using a Biospec Products Mini Bead Beater-16 (Klig *et al.*, 1985), and the protein A–tagged Nem1-Spo7 complex was eluted from IgG-Sepharose with 50 mM glycine-HCl (pH 3.0). The acid-eluted enzyme preparation was neutralized with 1 M Tris-HCl (pH 8.0) buffer, and the final preparation contained 160 mM Tris-HCl (pH 8.0), 0.02% Triton X-100, and 20% glycerol. The endogenously phosphorylated Pah1 was purified to near homogeneity from *S. cerevisiae* as described previously (O'Hara *et al.*, 2006). Nem1-Spo7 phosphatase activity was measured by following the shift in the electrophoretic mobility of Pah1 upon SDS–PAGE at 30°C. The reaction contained 15 ng of Pah1, 0.7 ng of Nem1-Spo7 phosphatase, 10 mM $MgCl_2$, 0.25 mM Triton X-100, 1 mM dithiothreitol, and 100 mM indicated buffers in a total volume of 50 μl. After 10-min incubation, the reaction product was analyzed by SDS–PAGE, followed by Western blot analysis using anti-Pah1 antibodies.

Labeling and analysis of lipids

Wild-type (BY4742) and mutant (4Δ, 4Δ *dgk1*Δ, 4Δ *pct1*Δ) strains were grown at 30°C from precultures at an OD of 0.1 for 17 and 19 h, respectively. Steady-state labeling of phospholipids and neutral lipids with ^{32}Pi and [2-^{14}C]acetate, respectively, was performed as described previously (Han *et al.*, 2006). The lipids were extracted by the method of Bligh and Dyer (1959). Part of the extract was subjected to one-dimensional (1D) TLC on silica gel 60 plates using the solvent system hexane/diethyl ether/acetic acid (40:10:1) to separate total phospholipids and neutral lipids (Henderson and Tocher, 1992). The other part of the extract was subjected to 1D TLC on Partisil LK6D silica gel 60 plates using the solvent system chloroform/ethanol/water/triethylamine (30:35:7:35) to separate the phospholipids (Vaden *et al.*, 2005). The identity of the labeled lipids on TLC plates was confirmed by comparison with standards after exposure to iodine vapor. Radiolabeled lipids were visualized by phosphorimaging and subjected to ImageQuant analysis.

Flow cytometry

BODIPY quantification by flow cytometry was performed as previously described (Gaspar *et al.*, 2008), with minor modifications. Briefly, cells were fixed for 30 min at room temperature with 3.7% formaldehyde, washed once with phosphate-buffered saline, and incubated with 10 μM BODIPY 493/503 for 10 min at room temperature. Cells were immediately analyzed on a FACSCalibur flow cytometer (BD Biosciences, San Jose, CA). Lipid droplet labeling was measured using the FL-1 detector, and the data were analyzed with FlowJo software, version 9 (Tree Star, Ashland, OR).

β-Galactosidase activity

Yeast cells expressing an *INO1-LacZ* reporter (pJH359; Lopes *et al.*, 1991) in 2% glucose SC medium followed by overnight growth in 2% raffinose SC medium were pelleted and resuspended into SC medium containing 2% galactose. Cells were grown for 7 h at 30°C, and β-galactosidase activity was measured as previously described (Reynolds *et al.*, 2001).

REFERENCES

Adeyo O, Horn PJ, Lee S, Binns DD, Chandrahas A, Chapman KD, Goodman JM (2011). The yeast lipin orthologue Pah1p is important for biogenesis of lipid droplets. J Cell Biol 192, 1043–1055.

Bahmanyar S, Biggs R, Schuh AL, Desai A, Müller-Reichert T, Audhya A, Dixon JE, Oegema K (2014). Spatial control of phospholipid flux restricts endoplasmic reticulum sheet formation to allow nuclear envelope breakdown. Genes Dev 28, 121–126.

Bligh EG, Dyer WJ (1959). A rapid method of total lipid extraction and purification. Can J Biochem Physiol 37, 911–917.

Campbell JL, Lorenz A, Witkin KL, Hays T, Loidl J, Cohen-Fix O (2006). Yeast nuclear envelope subdomains with distinct abilities to resist membrane expansion. Mol Biol Cell 17, 1768–1778.

Choi HS, Su WM, Han GS, Plote D, Xu Z, Carman GM (2012). Pho85p-Pho80p phosphorylation of yeast Pah1p phosphatidate phosphatase regulates its activity, location, abundance, and function in lipid metabolism. J Biol Chem 287, 11290–11301.

Choi HS, Su WM, Morgan JM, Han GS, Xu Z, Karanasios E, Siniossoglou S, Carman GM (2011). Phosphorylation of phosphatidate phosphatase regulates its membrane association and physiological functions in Saccharomyces cerevisiae: identification of Ser(602), Thr(723), and Ser(744) as the sites phosphorylated by CDC28 (CDK1)-encoded cyclin-dependent kinase. J Biol Chem 286, 1486–1498.

Cornell RB, Northwood IC (2000). Regulation of CTP:phosphocholine cytidylyltransferase by amphitropism and relocalization. Trends Biochem Sci 25, 441–447.

Csaki LS, Dwyer JR, Fong LG, Tontonoz P, Young SG, Reue K (2013). Lipins, lipodystrophy, and the modulation of cellular lipid storage and signaling. Prog Lipid Res 52, 305–316.

Currie E, Guo X, Christiano R, Chitraju C, Kory N, Harrison K, Haas J, Walther TC, Farese RV Jr (2014). High confidence proteomic analysis of yeast LDs identifies additional droplet proteins and reveals connections to dolichol synthesis and sterol acetylation. J Lipid Res 55, 1465–1477.

Dawaliby R, Mayer A (2010). Microautophagy of the nucleus coincides with a vacuolar diffusion barrier at nuclear-vacuolar junctions. Mol Biol Cell 21, 4173–4183.

Dechant R, Saad S, Ibáñez AJ, Peter M (2014). Cytosolic pH regulates cell growth through distinct GTPases, Arf1 and Gtr1, to promote Ras/PKA and TORC1 activity. Mol Cell 55, 409–421.

de Virgilio C (2012). The essence of yeast quiescence. FEMS Microbiol Rev 36, 306–339.

Donkor J, Sariahmetoglu M, Dewald J, Brindley DN, Reue K (2007). Three mammalian lipins act as phosphatidate phosphatases with distinct tissue expression patterns. J Biol Chem 282, 3450–3457.

Dubots E, Cottier S, Péli-Gulli MP, Jaquenoud M, Bontron S, Schneiter R, De Virgilio C (2014). TORC1 regulates Pah1 phosphatidate phosphatase activity via the Nem1/Spo7 protein phosphatase complex. PLoS One 9, e104194.

Eaton JM, Mullins GR, Brindley DN, Harris TE (2013). Phosphorylation of lipin 1 and charge on the phosphatidic acid head group control its phosphatidic acid phosphatase activity and membrane association. J Biol Chem 288, 9933–9945.

Eaton JM, Takkellapati S, Lawrence RT, McQueeney KE, Boroda S, Mullins GR, Sherwood SG, Finck BN, Villén J, Harris TE (2014). Lipin 2 binds phosphatidic acid by the electrostatic hydrogen bond switch mechanism independent of phosphorylation. J Biol Chem 289, 18055–18066.

Fakas S, Konstantinou C, Carman GM (2011). DGK1-encoded diacylglycerol kinase activity is required for phospholipid synthesis during growth resumption from stationary phase in Saccharomyces cerevisiae. J Biol Chem 286, 1464–1474.

Gaspar ML, Jesch SA, Viswanatha R, Antosh AL, Brown WJ, Kohlwein SD, Henry SA (2008). A block in endoplasmic reticulum-to-Golgi trafficking inhibits phospholipid synthesis and induces neutral lipid accumulation. J Biol Chem 283, 25735–25751.

Golden A, Liu J, Cohen-Fix O (2009). Inactivation of the C. elegans lipin homolog leads to ER disorganization and to defects in the breakdown and reassembly of the nuclear envelope. J Cell Sci 122, 1970–1978.

Gorjánácz M, Mattaj IW (2009). Lipin is required for efficient breakdown of the nuclear envelope in Caenorhabditis elegans. J Cell Sci 122, 1963–1969.

Griffith J, Mari M, De Maziere A, Reggiori F (2008). A cryosectioning procedure for the ultrastructural analysis and the immunogold labelling of yeast Saccharomyces cerevisiae. Traffic 9, 1060–1072.

Grimsey N, Han GS, O'Hara L, Rochford JJ, Carman GM, Siniossoglou S (2008). Temporal and spatial regulation of the phosphatidate phosphatases lipin 1 and 2. J Biol Chem 283, 29166–29174.

Han GS, O'Hara L, Carman GM, Siniossoglou S (2008). An unconventional diacylglycerol kinase that regulates phospholipid synthesis and nuclear membrane growth. J Biol Chem 283, 20433–20442.

Han GS, Wu WI, Carman GM (2006). The Saccharomyces cerevisiae Lipin homolog is a Mg^{2+}-dependent phosphatidate phosphatase enzyme. J Biol Chem 281, 9210–9218.

Harris TE, Huffman TA, Chi A, Shabanowitz J, Hunt DF, Kumar A, Lawrence JC Jr (2007). Insulin controls subcellular localization and multisite phosphorylation of the phosphatidic acid phosphatase, lipin 1. J Biol Chem 282, 277–286.

Henderson RJ, Tocher DR (1992). Thin-layer chromatography. In: Lipid Analysis, ed. RJ Hamilton and S Hamilton, New York: IRL Press, 65–111.

Hsieh LS, Su WM, Han GS, Carman GM (2015). Phosphorylation regulates the ubiquitin-independent degradation of yeast Pah1 phosphatidate phosphatase by the 20S proteasome. J Biol Chem 290, 11467–11478.

Huffman TA, Mothe-Satney I, Lawrence JC Jr (2002). Insulin-stimulated phosphorylation of lipin mediated by the mammalian target of rapamycin. Proc Natl Acad Sci USA 99, 1047–1052.

Jacquier N, Choudhary V, Mari M, Toulmay A, Reggiori F, Schneiter R (2011). Lipid droplets are functionally connected to the endoplasmic reticulum in Saccharomyces cerevisiae. J Cell Sci 124, 2424–2437.

Janke C, Magiera MM, Rathfelder N, Taxis C, Reber S, Maekawa H, Moreno-Borchart A, Doenges G, Schwob E, Schiebel E, Knop M (2004). A versatile toolbox for PCR-based tagging of yeast genes: new fluorescent proteins, more markers and promoter substitution cassettes. Yeast 21, 947–962.

Karanasios E, Barbosa AD, Sembongi H, Mari M, Han GS, Reggiori F, Carman GM, Siniossoglou S (2013). Regulation of lipid droplet and membrane biogenesis by the acidic tail of the phosphatidate phosphatase Pah1p. Mol Biol Cell 24, 2124–2133.

Karanasios E, Han GS, Xu X, Carman GM, Siniossoglou S (2010). A phosphorylation-regulated amphipathic helix controls the membrane translocation and function of the yeast phosphatidate phosphatase. Proc Natl Acad Sci USA 107, 17539–17544.

Klig LS, Homann MJ, Carman GM, Henry SA (1985). Coordinate regulation of phospholipid biosynthesis in Saccharomyces cerevisiae: pleiotropically constitutive opi1 mutant. J Bacteriol 162, 1135–1141.

Kohlwein SD, Eder S, Oh CS, Martin CE, Gable K, Bacikova D, Dunn T (2001). Tsc13p is required for fatty acid elongation and localizes to a novel structure at the nuclear-vacuolar interface in Saccharomyces cerevisiae. Mol Cell Biol 21, 109–125.

Kohlwein SD, Veenhuis M, van der Klei IJ (2013). Lipid droplets and peroxisomes: key players in cellular lipid homeostasis or a matter of fat—store 'em up or burn 'em down. Genetics 193, 1–50.

Kooijman EE, Tieleman DP, Testerink C, Munnik T, Rijkers DT, Burger KN, de Kruijff B (2007). An electrostatic/hydrogen bond switch as the basis for the specific interaction of phosphatidic acid with proteins. J Biol Chem 282, 11356–11364.

Kvam E, Goldfarb DS (2007). Nucleus-vacuole junctions and piecemeal microautophagy of the nucleus in S. cerevisiae. Autophagy 3, 85–92.

Levine TP, Munro S (2001). Dual targeting of Osh1p, a yeast homologue of oxysterol-binding protein, to both the Golgi and the nucleus-vacuole junction. Mol Biol Cell 12, 1633–1644.

Longtine MS, McKenzie A 3rd, Demarini DJ, Shah NG, Wach A, Brachat A, Philippsen P, Pringle JR (1998). Additional modules for versatile and economical PCR-based gene deletion and modification in Saccharomyces cerevisiae. Yeast 14, 953–961.

Lopes JM, Hirsch JP, Chorgo PA, Schulze KL, Henry SA (1991). Analysis of sequences in the INO1 promoter that are involved in its regulation by phospholipid precursors. Nucleic Acids Res 19, 1687–1693.

MacKinnon MA, Curwin AJ, Gaspard GJ, Suraci AB, Fernández-Murray JP, McMaster CR (2009). The Kap60-Kap95 karyopherin complex directly regulates phosphatidylcholine synthesis. J Biol Chem 284, 7376–7384.

Mall M, Walter T, Gorjánácz M, Davidson IF, Nga Ly-Hartig TB, Ellenberg J, Mattaj IW (2012). Mitotic lamin disassembly is triggered by lipid-mediated signaling. J Cell Biol 198, 981–990.

Mollapour M, Shepherd A, Piper PW (2008). Novel stress responses facilitate Saccharomyces cerevisiae growth in the presence of the monocarboxylate preservatives. Yeast 25, 169–177.

Oelkers P, Cromley D, Padamsee M, Billheimer JT, Sturley SL (2002). The DGA1 gene determines a second triglyceride synthetic pathway in yeast. J Biol Chem 277, 8877–8881.

Orij R, Urbanus ML, Vizeacoumar FJ, Giaever G, Boone C, Nislow C, Brul S, Smits GJ (2012). Genome-wide analysis of intracellular pH reveals quantitative control of cell division rate by pH(c) in Saccharomyces cerevisiae. Genome Biol 13, R80.

O'Hara L, Han GS, Peak-Chew S, Grimsey N, Carman GM, Siniossoglou S (2006). Control of phospholipid synthesis by phosphorylation of the yeast lipin Pah1p/Smp2p Mg^{2+}-dependent phosphatidate phosphatase. J Biol Chem 281, 34537–34548.

Pan X, Roberts P, Chen Y, Kvam E, Shulga N, Huang K, Lemmon S, Goldfarb DS (2000). Nucleus-vacuole junctions in Saccharomyces cerevisiae are formed through the direct interaction of Vac8p with Nvj1p. Mol Biol Cell 11, 2445–2457.

Pascual F, Carman GM (2013). Phosphatidate phosphatase, a key regulator of lipid homeostasis. Biochim Biophys Acta 1831, 514–522.

Pascual F, Hsieh LS, Soto-Cardalda A, Carman GM (2014). Yeast Pah1p phosphatidate phosphatase is regulated by proteasome-mediated degradation. J Biol Chem 289, 9811–9822.

Peterfy M, Phan J, Xu P, Reue K (2001). Lipodystrophy in the fld mouse results from mutation of a new gene encoding a nuclear protein, lipin. Nat Genet 27, 121–124.

Petschnigg J, Wolinski H, Kolb D, Zellnig G, Kurat CF, Natter K, Kohlwein SD (2009). Good fat, essential cellular requirements for triacylglycerol synthesis to maintain membrane homeostasis in yeast. J Biol Chem 284, 30981–30993.

Pol A, Gross SP, Parton RG (2014). Biogenesis of the multifunctional lipid droplet: lipids, proteins, and sites. J Cell Biol 204, 635–646.

Reynolds A, Lundblad V, Dorris D, Keaveney M (2001). Yeast vectors and assays for expression of cloned genes. Curr Protoc Mol Biol Chapter 13, Unit 13.6.

Santos-Rosa H, Leung J, Grimsey N, Peak-Chew S, Siniossoglou S (2005). The yeast lipin Smp2 couples phospholipid biosynthesis to nuclear membrane growth. EMBO J 24, 1931–1941.

Shin JJ, Loewen CJ (2011). Putting the pH into phosphatidic acid signaling. BMC Biol 9, 85.

Siniossoglou S (2009). Lipins, lipids and nuclear envelope structure. Traffic 10, 1181–1187.

Siniossoglou S, Hurt EC, Pelham HR (2000). Psr1p/Psr2p, two plasma membrane phosphatases with an essential DXDX(T/V) motif required for sodium stress response in yeast. J Biol Chem 275, 19352–19360.

Siniossoglou S, Santos-Rosa H, Rappsilber J, Mann M, Hurt E (1998). A novel complex of membrane proteins required for formation of a spherical nucleus. EMBO J 17, 6449–6464.

Su WM, Han GS, Carman GM (2014). Yeast Nem1-Spo7 protein phosphatase activity on Pah1 phosphatidate phosphatase is specific for the Pho85-Pho80 protein kinase phosphorylation sites. J Biol Chem 289, 34699–34708.

Su WM, Han GS, Casciano J, Carman GM (2012). Protein kinase A-mediated phosphorylation of Pah1p phosphatidate phosphatase functions in conjunction with the Pho85p-Pho80p and Cdc28p-cyclin B kinases to regulate lipid synthesis in yeast. J Biol Chem 287, 33364–33376.

Tange Y, Hirata A, Niwa O (2002). An evolutionarily conserved fission yeast protein, Ned1, implicated in normal nuclear morphology and chromosome stability, interacts with Dis3, Pim1/RCC1 and an essential nucleoporin. J Cell Sci 115, 4375–4385.

Thomas BJ, Rothstein R (1989). Elevated recombination rates in transcriptionally active DNA. Cell 56, 619–630.

Toulmay A, Prinz WA (2013). Direct imaging reveals stable, micrometer-scale lipid domains that segregate proteins in live cells. J Cell Biol 202, 35–44.

Vaden DL, Gohil VM, Gu Z, Greenberg ML (2005). Separation of yeast phospholipids using one-dimensional thin-layer chromatography. Anal Biochem 338, 162–164.

Wang CW, Lee SC (2012). The ubiquitin-like (UBX)-domain-containing protein Ubx2/Ubxd8 regulates lipid droplet homeostasis. J Cell Sci 125, 2930–2939.

Wang CW, Miao YH, Chang YS (2014). A sterol-enriched vacuolar microdomain mediates stationary phase lipophagy in budding yeast. J Cell Biol 206, 357–366.

Wimmer C, Doye V, Grandi P, Nehrbass U, Hurt EC (1992). A new subclass of nucleoporins that functionally interact with nuclear pore protein NSP1. EMBO J 11, 5051–5061.

Witkin KL, Chong Y, Shao S, Webster MT, Lahiri S, Walters AD, Lee B, Koh JL, Prinz WA, Andrews BJ, Cohen-Fix O (2012). The budding yeast nuclear envelope adjacent to the nucleolus serves as a membrane sink during mitotic delay. Curr Biol 22, 1128–1133.

Yen CL, Stone SJ, Koliwad S, Harris C, Farese RV Jr (2008). Thematic review series: glycerolipids. DGAT enzymes and triacylglycerol biosynthesis. J Lipid Res 49, 2283–2301.

Yorimitsu T, Zaman S, Broach JR, Klionsky DJ (2007). Protein kinase A and Sch9 cooperatively regulate induction of autophagy in Saccharomyces cerevisiae. Mol Biol Cell 18, 4180–4189.

Zhang P, Verity MA, Reue K (2014). Lipin-1 regulates autophagy clearance and intersects with statin drug effects in skeletal muscle. Cell Metab 20, 267–279.